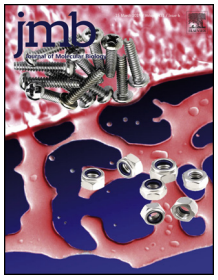

Characterization of Mitochondrial YME1L Protease Oxidative Stress-Induced Conformational State

Chad A. Brambley, Justin D. Marsee, Neal Halper and Justin M. Miller

Department of Chemistry, *Middle Tennessee State University, 1301 East Main Street, Murfreesboro, TN 37132, USA*

Correspondence to Justin M. Miller: *Justin.Miller@mtsu.edu*
https://doi.org/10.1016/j.jmb.2019.01.039
Edited by Yigong Shi

Abstract

Oxidative stress is a common challenge to mitochondrial function where reactive oxygen species are capable of significant organelle damage. The generation of mitochondrial reactive oxygen species occurs in the inner membrane and matrix compartments as a consequence of subunit function in the electron transport chain and citric acid cycle, respectively. Maintenance of mitochondrial proteostasis and stress response is facilitated by compartmentalized proteases that couple the energy of ATP hydrolysis to unfolding and the regulated removal of damaged, misfolded, or aggregated proteins. The mitochondrial protease YME1L functions in the maintenance of proteostasis in the intermembrane space. YME1L is an inner membrane-anchored hexameric protease with distinct N-terminal, transmembrane, AAA+ (ATPases associated with various cellular activities), and C-terminal M41 zinc-dependent protease domains. The effect of oxidative stress on enzymes such as YME1L tasked with maintaining proteostasis is currently unclear. We report here that recombinant YME1L undergoes a reversible conformational change in response to oxidative stress that involves the interaction of one hydrogen peroxide molecule per YME1L monomer with affinities equal to 31 ± 2 and 26 ± 1 mM for conditions lacking or including nucleotide, respectively. Our data also reveal that oxidative stress does not significantly impact nucleotide binding equilibria, but does stimulate a 2-fold increase in the rate constant for high-affinity ATP binding from $(8.9 \pm 0.2) \times 10^5$ M^{-1} s^{-1} to $(1.5 \pm 0.1) \times 10^6$ M^{-1} s^{-1}. Taken together, these data may suggest a mechanism for the regulated processing of YME1L by other inner membrane proteases such as OMA1.

Introduction

Mitochondria are an essential organelle that determines the life and death of eukaryotic cells. They are critical for required cellular processes such as oxidative phosphorylation, biomolecular synthesis, calcium homeostasis, and apoptosis [1]. Damage to mitochondrial elements necessary for function can produce severe phenotypes in tissues with higher energy demands such as the heart, brain, and skeletal muscle [2]. Mitochondrial dysfunction related to defects in proteins encoded by the mitochondrial genome lead to respiratory defects that exhibit broad variability with respect to clinically observed phenotypes and often progressively worsen with age.

The prevailing models describing organismal aging mechanisms suggest that chronic exposure to mitochondrial reactive oxygen species (mROS) can lead to the damage of critical biomolecules that include lipids, proteins, and the mitochondrial genome. mROS species include highly reactive molecules such as superoxide ($\bullet O_2^-$), hydroxyl radical (•OH), and hydrogen peroxide (H_2O_2). The production of mROS occurs in the mitochondrial inner membrane and matrix compartments as a consequence of the normal function of subunits within the electron transport chain (ETC) and the citric acid cycle, respectively [3–5]. Electron leakage in the ETC at complexes I and III can support semiubiquinone radical reaction with oxygen to form superoxide [5]. Under normal conditions, mROS production correlates positively with mitochondrial membrane potential such that decreasing the inner mitochondrial membrane potential leads to decreased mROS production [6]. Dissipation of the mitochondrial proton gradient by uncoupling proteins (UCP1–5) may serve as an antioxidant mechanism to protect against mROS accumulation via ETC regulation

[7,8]. Decreasing the inner mitochondrial membrane potential decreases the thermodynamic barrier associated with terminal electron transfer to oxygen, thus minimizing the possibility of electron loss leading to superoxide production. Pathological mROS concentrations are observed when mROS production is not balanced by endogenous scavenging systems and ETC regulation [9]. Oxidative conditions can promote a cascade-like series of events leading to mitochondrial damage and increased mROS formation.

To avoid deleterious effects associated with accumulated mitochondrial damage, the equilibrium between mitochondrial fusion and fission is strictly regulated. Fusion of mitochondria allows for the mixing and dilution of mutant and wild-type mitochondrial gene products [10]. Mitochondrial fusion involves the separate merging of the outer and inner mitochondrial membranes. Fusion of the outer mitochondrial membrane is a homotypic event involving symmetric interactions between outer membrane mitofusion proteins, whereas inner-membrane fusion requires heterotypic interactions between the dynamin-like 120-kDa guanosine triphosphatase, also known as optic atrophy 1 (OPA1), and cardiolipin [11–15]. Mammalian OPA1 exists as an inner membrane-associated "long-form" (L-OPA1) and a soluble "short-form" (S-OPA1) [15]. S-OPA1 is generated through proteolytic cleavage of L-OPA1 catalyzed by the inner membrane-associated YME1L and OMA1 zinc-metalloproteases [13–15]. Owing to its association with the inner membrane, L-OPA1 is necessary for mitochondrial fusion, whereas S-OPA1 accumulation promotes fission and a fragmented mitochondrial network [1,13,15,16].

The proteolytic activities of YME1L and OMA1 toward OPA1 are reciprocally controlled under conditions of oxidative stress [17,18]. When [ATP] is high under oxidative conditions, OMA1 is degraded as a substrate by YME1L. In contrast, significant depletion of the mitochondrial ATP pool under oxidative stress conditions promotes OMA1 activation and OMA1 catalyzed degradation of YME1L [17,19]. Oxidative stress-induced activation of OMA1 also leads to the rapid conversion of L-OPA1 to S-OPA1, which favors mitochondrial fragmentation via fission [13,16–18]. Stress-induced fragmentation may ultimately lead to PINK1/Parkin-dependent ubiquitination of outer-membrane proteins, thereby positioning fragmented mitochondria for removal by mitophagy [14].

Healthy cells must balance the production of the long- and short-OPA1 isoforms to maintain normal mitochondrial morphology. This balance is dependent on proper function of the ATP-dependent YME1L protease since YME1L/OMA1 dynamics are central to the regulation of S-OPA1 production. Deletion of the *YME1L* gene has been observed to result in dilated cardiomyopathy and heart failure in aged mice associated with increased S-OPA1 production by OMA1 [16]. This phenotype is reversed upon deletion of both OMA1 and YME1L where mitochondrial morphology and normal heart function are restored. Taken together, these data strongly suggest that mROS accumulation may directly impact mitochondrial dynamics by activation of OMA1. However, the impact of mROS on the mitochondrial AAA+ YME1L protease remains unclear. The potential for mROS-dependent effects on YME1L function represents a significant area of research that has been understudied at the current time.

YME1L is anchored to the mitochondrial inner membrane via an insoluble transmembrane segment. This structural arrangement projects AAA+ ATPase and M41 protease domains into the intermembrane space. Shi and coworkers [20] have recently reported a method that allows for the recombinant expression of soluble YME1L AAA+ and M41 domains suitable for use in biochemical studies. In that work, the soluble YME1L domains were expressed as a fusion bearing an N-terminal cc-Hex sequence sufficient to drive the formation of hexamers with high ATPase and proteolytic activities [21]. Here, we have utilized this methodology to investigate the enzymatic behavior of YME1L under conditions of oxidative stress. We report that recombinant YME1L adopts unique conformational states that depend on the presence of nucleotide and oxidative stress. Our data demonstrate that oxidative stress leads to an increase in the rate of ATP binding, but does not significantly impact YME1L catalyzed protein unfolding over all conditions examined here. Moreover, our data reveal that ATP binding by YME1L occurs with negative cooperativity. Based on this, we propose that condition-dependent YME1L conformational states may facilitate recognition by OMA1. Taken together, YME1L conformational dynamics may dictate whether YME1L serves as a substrate for OMA1 or whether the inverse occurs.

Results

YME1L undergoes reversible oxidative stress-related conformational changes

The relationship between YME1L conformation and function under oxidative stress conditions is currently unclear. To determine how YME1L conformational dynamics are impacted by oxidative stress, we performed a set of limited proteolysis experiments wherein 3 μM YME1L was incubated with 25 nM proteinase K at 25 °C for 1 h in the presence and absence of 200 mM H_2O_2. Samples were taken at 10-min intervals, quenched with SDS-sample loading buffer supplemented with 10 mM PMSF, and prepared for analysis by SDS-PAGE. Digestion products were then visualized by coomassie staining on a 10% acrylamide gel. Figure 1A–B demonstrates

that solution conditions differing only in the presence of 200 mM H_2O_2 yield significantly different proteinase K-dependent digestion rates of YME1L. Intact YME1L persists for at least 50 min in the absence of H_2O_2 (Fig. 1A), whereas oxidative conditions sensitize YME1L such that complete proteinase K-dependent digestion is complete within 30 min (Fig. 1B). Control experiments reporting on degradation of an unrelated protein substrate demonstrate that hydrogen peroxide does not influence proteinase K proteolytic activity (Fig. S1). These data strongly suggest that YME1L undergoes a conformational change upon introduction of oxidative stress to yield a three-dimensional structure that is readily degraded by proteinase K.

In vivo oxidation of proteins is known to represent a mechanism that may lead to the regulation of enzyme function. Common oxidation events can occur reversibly via disulfide formation or *S*-glutathionylation as well as irreversibly by covalent modification of amino acid side-chains that include arginine, lysine, histidine, and cysteine. To examine whether differences in YME1L conformation observed in Fig. 1A–B are reversible, we modified the experimental strategy discussed above. Independent YME1L (3 μM) samples were incubated for 1 h under conditions lacking or including 200 mM H_2O_2. After incubation, both samples were subjected to extensive dialysis into fresh H150 buffer (Materials and Methods) to remove any residual hydrogen peroxide. Each dialyzed sample was then incubated in the presence of 25 nM proteinase K for 50 min as described above. Samples were again taken at 10-min intervals, quenched with SDS-Sample loading buffer supplemented with 10 mM PMSF, and prepared for analysis by SDS-PAGE. The control experiment presented in Fig. 1C illustrates that YME1L is stable during this experimental protocol such that non-oxidative conditions yield a conformation with sensitivity to proteinase K digestion that is qualitatively similar to the data shown in Fig. 1A.

Figure 1D represents the result of an experimental design where YME1L has been treated with 200 mM H_2O_2 and extensively dialyzed. Figure 1D reveals that YME1L does not display significant sensitivity to proteinase K digestion after dialysis such that starting material persists for at least 50 min, which contrasts the data presented in Fig. 1B. The qualitative differences between Fig. 1B and D may indicate reversibility in YME1L:H_2O_2 interactions at allosteric sites that drive conformational dynamics. It is highly unlikely that YME1L undergoes no irreversible oxidation under these conditions. Analysis of the YME1L primary sequence (hexYME1L construct) indicates the presence of 24 arginine, 1 cysteine, 9 histidine, and 41 lysine residues, which are all known to undergo irreversible oxidative chemistry [22–25]. Figure 1E highlights the position of each of these residue types in a YME1L hexamer homology model

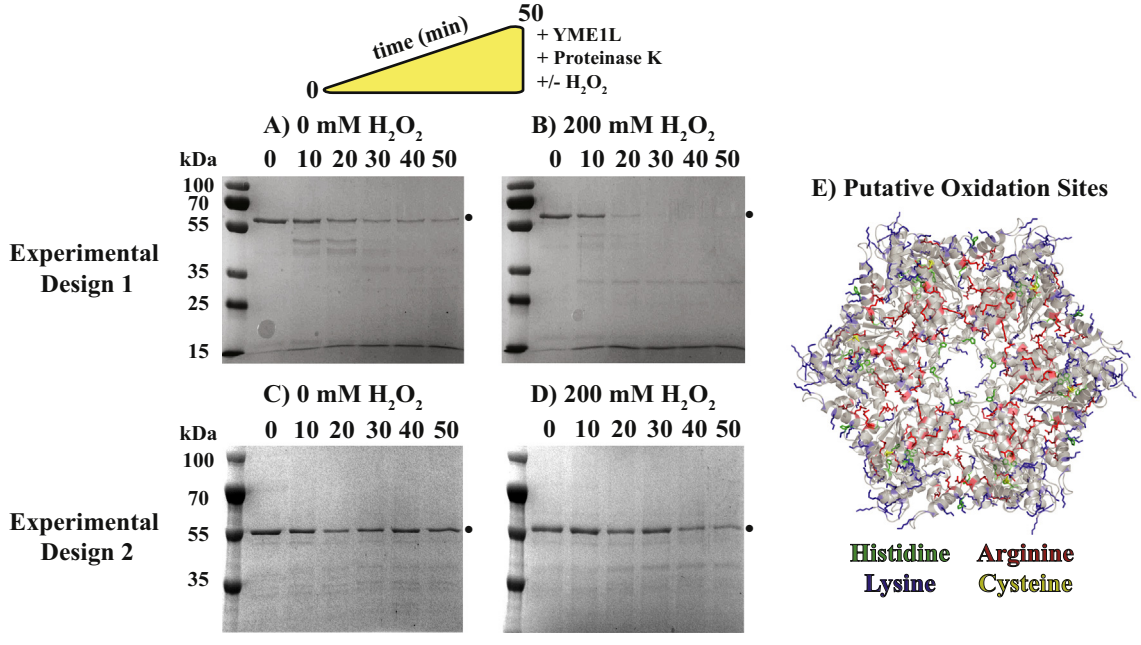

Fig. 1. YME1L undergoes a conformational change in the presence of oxidative stress. YME1L (3 μM) was incubated at 25 °C with 25 nM proteinase K for 50 min in the absence (A) and presence (B) of 200 mM H_2O_2. Samples were taken at 10-min intervals and subjected to analysis by SDS-PAGE. Gel bands that correspond to intact YME1L are marked by a dot. YME1L starting material is observed to persist for at least 50 min in the absence of H_2O_2 (A). In contrast, YME1L exhibits increased sensitivity to proteinase K under oxidative stress (B) such that starting material is not observed after 30 min in the presence of 200 mM H_2O_2.

constructed using the SWISS-MODEL server [26–30]. Residues are colored as green, blue, red, or yellow to indicate the position of histidine, lysine, arginine, or cysteine, respectively. Given the uniform distribution of residues prone to oxidation, the conformational reversibility shown in Fig. 1D suggests that a subset of YME1L:H_2O_2 interactions may involve non-covalent interactions that likely occur at allosteric sites related to conformational control. However, the molecular details underlying such conformational events are currently unclear.

YME1L conformational changes are [ATPγS]-dependent

Given the known [ATP] dependence of the YME1L/OMA1 reciprocal proteolytic relationship, we next sought to determine the impact of nucleotide on YME1L conformation. Limited proteolysis experiments were performed using experimental design 1 (Fig. 1A and B) in the absence of H_2O_2 and in the presence of varied concentrations of ATPγS ranging from 0 to 3 mM ATPγS (Fig. 2A), where the reported Michaelis constant describing YME1L catalyzed ATP hydrolysis is equal to 1.4 mM [20]. As reported in Fig. 1A, intact YME1L persists in the presence of proteinase K for at least 50 min in the absence of nucleotide and H_2O_2. Figure 2A demonstrates that incremental increases in [ATPγS] promote increased proteinase K-dependent digestion of YME1L. YME1L digestion is complete after 40, 30, and 20 min in the presence of 0.5, 1.4, and 3 mM ATPγS, respectively. This observation suggests an [ATPγS]-dependent continuum with a transition from an apo or nucleotide-subsaturated conformational state to a separate conformation corresponding to nucleotide-saturated YME1L at elevated nucleotide concentrations. Figure 2B reveals that, in the presence of 200 mM H_2O_2, increasing [ATPγS] from 0 to 3 mM promotes a similar trend in proteinase K-dependent YME1L digestion as observed under non-oxidative conditions in SDS-PAGE experiments. However, oxidative conditions that include 0.25 or 0.5 mM ATPγS yield a YME1L population with an average conformation similar to the apo or nucleotide-subsaturated non-oxidative states as concluded qualitatively from the starting material digestion rate. Comparison of conditions that include 0.5 mM ATPγS demonstrate that no starting material is observed after a 40-min incubation under non-oxidative conditions (Fig. 2A), whereas intact YME1L persists for at least 50 min under oxidative conditions (Fig. 2B).

Proteinase K-dependent YME1L digestion profiles observed in SDS-PAGE experiments suggest unique YME1L conformational states in the absence of nucleotide *versus* conditions including saturating [nucleotide]. Incubation of YME1L with proteinase K under oxidative conditions in the absence of ATPγS yields no significantly populated intermediates and a terminal digestion product after 50 min with an estimated molecular weight equal to 31.4 kDa. In contrast, the same experiment performed in the presence of 3 mM ATPγS produces an intermediate species after approximately 10 min with an estimated molecular weight equal to 43.1 kDa, which disappears after approximately 50 min to yield a terminal digestion product with estimated molecular weight equal to 36.6 kDa. These data suggest that YME1L adopts conformational states that are nucleotide dependent. Taken together, these data suggest distinct conformational states under oxidative conditions that populate according to nucleotide concentration, and correspond to apo-, nucleotide subsaturated-, and nucleotide saturated-states. Intermediate nucleotide concentrations likely promote a hybrid arrangement where hexamer units subsaturated with nucleotide adopt a conformational state composed of a mixture of apo and ATP-like conformations.

To quantitatively characterize H_2O_2-induced YME1L conformational changes, we performed a series of titrations reporting on the quenching of YME1L tryptophan residues by the ROS H_2O_2 [31]. In this experimental strategy, quencher-accessible tryptophan residues undergo [H_2O_2]-dependent quenching. Conformational changes associated with changing solvent conditions or nucleotide may result in corresponding changes in the quencher accessibility of YME1L tryptophan residues. A fluorescence spectrum collected in the absence of H_2O_2 or nucleotide indicates that these tryptophan residues are not equally accessible to solvent as indicated by the asymmetric emissions profile with peaks at 345 and 333 nm (Fig. 3A, red trace). The observation of separate emissions peaks that are each unstructured is consistent with tryptophan populations that reside in environments differing in solvent accessibility or hydrogen bonding via the indole imino group [32]. However, neither tryptophan population is expected to be shielded from hydrogen bonding since each peak is unstructured with maxima that do not reflect a blue shift consistent with a completely apolar environment.

Titration of 1 μM YME1L with incrementally increased [H_2O_2] strongly suggests non-uniform quencher accessibility among YME1L tryptophan residues. Figure 3A demonstrates a decrease in the observed fluorescence intensity at 345 nm as [H_2O_2] is increased such that the dominant peak observed at [H_2O_2] = 200 mM occurs at 333 nm. These observations are reproduced in the presence of 1.4 mM ATPγS and differ in the degree of quenching observed at 200 mM H_2O_2 (Fig. 3B). The data presented in Fig. 3A–B strongly suggest the presence of a tryptophan population that is shielded from solvent in the presence and absence of nucleotide. The unstructured emission peak observed at 333 nm in the presence of 200 mM H_2O_2 indicates

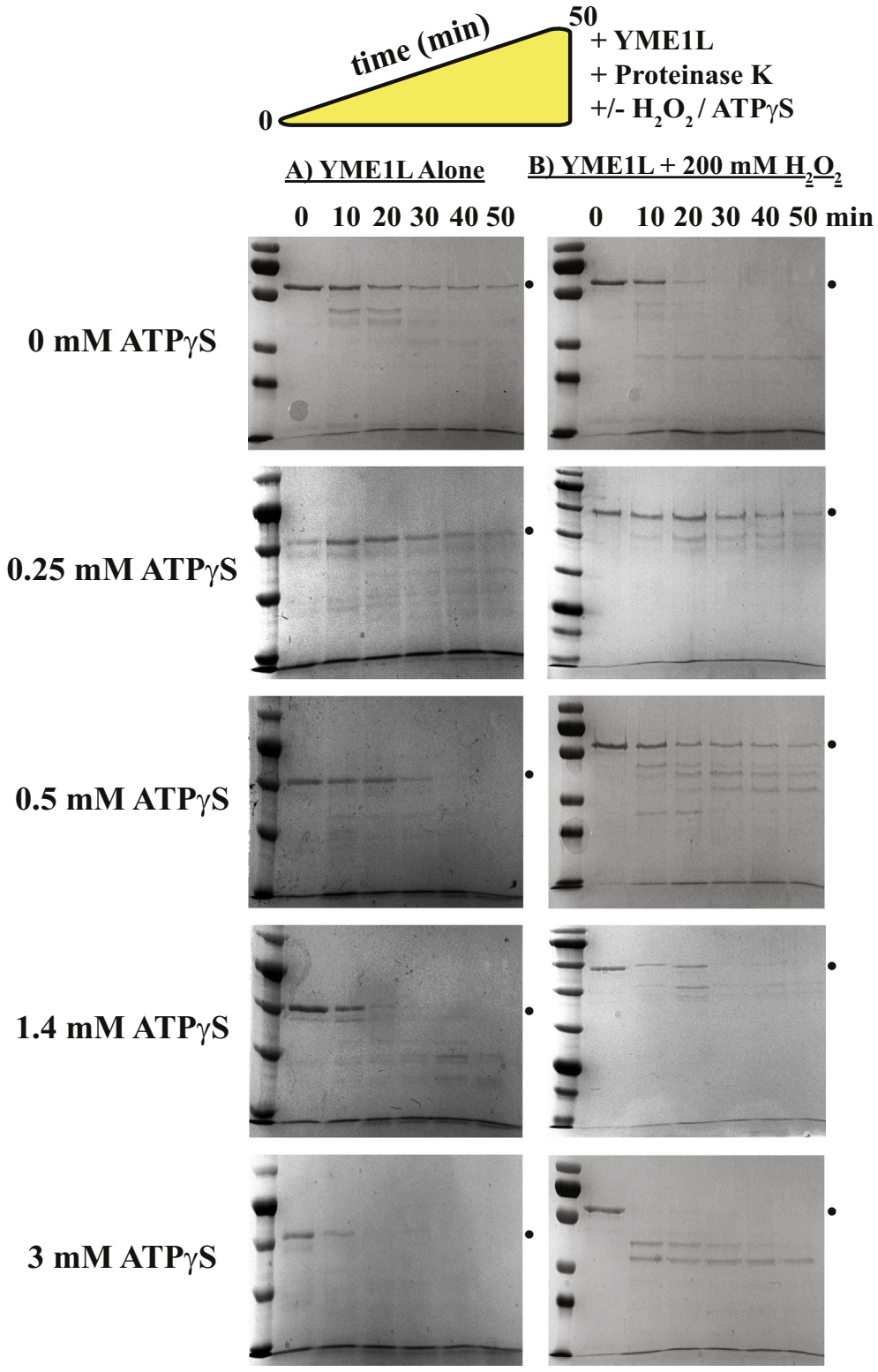

Fig. 2. Nucleotide binding to YME1L promotes conformational changes. YME1L (3 μM) was incubated at 25 °C in the presence of 25 nM proteinase K for 50 min in the absence (A) and presence (B) of 200 mM H_2O_2 and [ATPγS] equal to 0, 0.25, 0.5, 1.4, or 3 mM. Samples were taken at 10-min intervals and subjected to analysis by SDS-PAGE. Gel bands that correspond to intact YME1L are marked by a dot. (A–B) YME1L exhibits [ATPγS]-dependent sensitivity to proteinase K digestion independent of H_2O_2, consistent with a [nucleotide]-dependent YME1L conformational change.

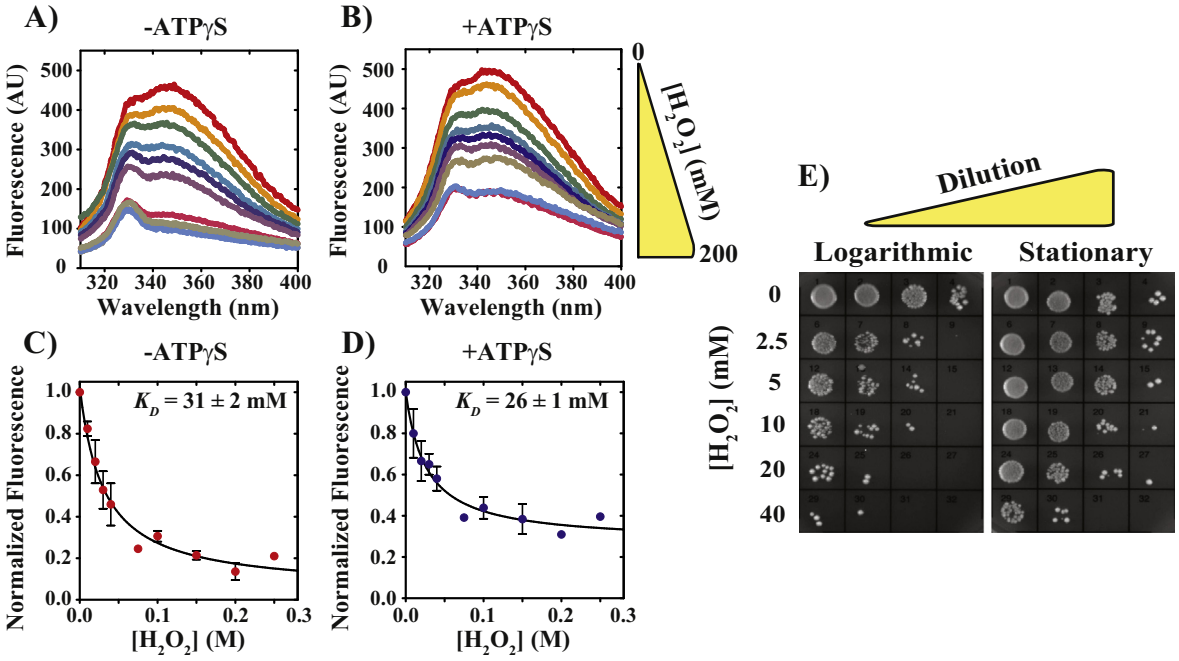

Fig. 3. (A–B) YME1L emissions spectra were collected in the presence of systematically varied concentrations of hydrogen peroxide in the absence (A) and presence (B) of 1.4 mM ATPγS. In the absence of quencher, emissions maxima are observed at 345 and 333 nm. (C) Dependence of normalized fluorescence observed at 345 nm on $[H_2O_2]$ in the absence of ATPγS, where the continuous line is the result of an NLLS fit to the Hill function with n_H constrained to equal one for A_{app} = 0.98 ± 0.06 and $K_{D,app}$ = 31 ± 2 mM. (D) Dependence of normalized fluorescence observed at 345 nm on $[H_2O_2]$ in the presence of ATPγS, where the continuous line is the result of an NLLS fit to the Hill function with n_H constrained to equal one for A_{app} = 0.73 ± 0.05 and $K_{D,app}$ = 26 ± 1 mM. All data represent average values determined from at least three independent experiments. Error bars indicate ± standard deviation. (E) Yeast viability after H_2O_2-treatment for logarithmic *versus* stationary phase cells was assessed in a serial dilution assay. All strains grown to stationary phase exhibited increased viability after oxidative treatment relative to logarithmic phase cells.

that this tryptophan population is likely hydrogen bonded in a quencher-inaccessible environment that must correspond to the protein interior.

Plots of normalized fluorescence *versus* hydrogen peroxide concentration in the absence and presence of 1.4 mM ATPγS are presented in Fig. 3C–D, respectively. Qualitative analysis of the data presented in Fig. 3C–D suggests a hyperbolic dependence of fluorescence quenching on $[H_2O_2]$. Preliminary nonlinear least squares (NLLS) fits of these data to a Hill function, shown as Eq. (2), yield estimates of the Hill coefficient as 1.5 ± 0.3 and 1.1 ± 0.3 for conditions lacking or including ATPγS, respectively. The observation of a Hill coefficient equal to 1.5 suggests that 1–2 hydrogen peroxide molecules interact per YME1L monomer to support the conformational change observed in Fig. 2A–B. However, the hyperbolic dependence of fluorescence quenching on $[H_2O_2]$ suggests a 1:1 interaction stoichiometry. As such, additional analyses of the data were performed with the Hill coefficient constrained to equal unity. The solid line presented in Fig. 3C is the result of an NLLS fit of quenching data collected in the absence of ATPγS to Eq. (2) with n_H constrained equal one for $K_{D,app}$ = 31 ± 2 mM and A_{app} = 0.98 ± 0.06. The Hill coefficient, apparent dissociation equilibrium constant, and apparent amplitude are denoted as n_H, $K_{D,app}$, and A_{app}, respectively. Similarly, constrained NLLS analysis of tryptophan quenching data collected in the presence of 1.4 mM ATPγS (Fig. 3D) estimates $K_{D,app}$ and A_{app} as 26 ± 1 mM and 0.73 ± 0.05, respectively. These fit parameters collectively suggest that the YME1L:H_2O_2 interaction is noncooperative such that one hydrogen peroxide molecule interacts per YME1L monomer independent of any bound nucleotide. However, the accessibility of YME1L tryptophan residues to hydrogen peroxide may depend on nucleotide binding, which is consistent with a nucleotide-dependent conformational change. The apparent amplitudes estimated in the absence *versus* presence of ATPγS are 0.98 ± 0.06 and 0.73 ± 0.05, respectively, which suggests a 25% decrease in quenching when nucleotide is present. Taken together alongside limited proteolysis data shown in Fig. 2A–B, these data suggest that nucleotide binding does not significantly impact the affinity describing the YME1L:H_2O_2 interaction, but may induce a conformational change that results in an altered population of quencher-accessible tryptophan residues.

To determine whether the apparent dissociation equilibrium constants observed in tryptophan quenching experiments are physiologically relevant, we performed phenotypic experiments to determine yeast viability under conditions of varied oxidative stress. The human YME1L homolog has previously been reported to functionally complement *yme1* gene disruptant yeast strains [33]. As such, similar function and stability may be expected for yeast Yme1p relative to its human YME1L homolog. Wild-type *Saccharomyces cerevisiae* were first grown in YPD media to either mid-logarithmic or stationary phase. After correction to a common OD_{600} = 0.5 in 0.1 M Hepes buffer (pH 7.5), yeast were exposed to [H_2O_2] ranging from 0 to 40 mM for 1 h. Following this incubation, cells were then harvested by centrifugation and washed with 0.1 M Hepes buffer to remove any residual H_2O_2. Aliquots were plated on YPD-agar medium as a dilution series and allowed to grow at 30 °C for 2–3 days. This protocol was utilized in order to compare wild-type *S. cerevisiae* alongside *yme1* and *oma1* gene disruptant strains. Figure 3E demonstrates that yeast grown to logarithmic phase exhibit decreased tolerance to H_2O_2 relative to stationary phase cells. However, no significant differences are observed in viability between wild-type, Δ*yme1*, and Δ*oma1* yeast strains when comparing cells grown to the same phase (data not shown). Figure 3E clearly illustrates that yeast are capable of surviving acute oxidative stress represented by [H_2O_2] up to at least 40 mM.

Oxidative stress does not significantly impact YME1L catalyzed protein unfolding

To determine whether [H_2O_2]-dependent YME1L conformational changes impact protein unfolding activities, we performed stopped-flow fluorescence experiments using a method that reports on YME1L catalyzed unfolding of a fluorescent protein [34,35]. Figure 4A illustrates the experimental design as described in the Materials and Methods section. Nucleotide-bound YME1L hexamers are preassembled with a fluorescent protein substrate bound and rapidly mixed in a stopped-flow spectrometer with an excess concentration of ATP to initiate the reaction. Syringe A of the stopped-flow spectrophotometer contains a solution of 1 μM YME1L, 0.5 mM ATPγS, and 500 nM photoactivated Kaede expressed with a C-terminal SsrA degradation sequence (SsrA-$Kaede_{Red}$). Thus, the contents of Syringe A represent a pre-assembled YME1L complex pre-bound to a protein substrate and stabilized by bound nucleotide. Upon mixing with 9.5 mM ATP in Syringe B, YME1L is expected to catalyze SsrA-$Kaede_{Red}$ unfolding and subsequent degradation. The representative time courses shown in Fig. 4B illustrate that the rapid mixing of the contents of the two syringes as shown in Fig. 4A results in a decrease in observed emissions at wavelengths above 570 nm as YME1L catalyzes SsrA-$Kaede_{Red}$ unfolding.

All time courses presented in Fig. 4B are biphasic, which is consistent with our experimental strategy described above. Because YME1L is initially pre-bound to SsrA-$Kaede_{Red}$, the initial rapid phase must correspond to a kinetic step involved in protein unfolding that occurs after the initial protein substrate binding event. In contrast, we predict the slower phase that follows to represent secondary cycles of YME1L catalyzed unfolding, which may be rate-limited by any kinetic step along the protein unfolding pathway. NLLS analysis of each time course yields estimates of the apparent rate constant for each phase (Fig. 4C). For clarity, we have labeled apparent rate constants corresponding to the initial rapid phase and the subsequent slow phase as k_1 and k_2, respectively. NLLS parameters are summarized in Table S1. Time courses collected at any [H_2O_2] shown here yield values for k_1 and k_2 that are statistically different from one another, which strongly suggests different rate-limiting steps in the initial *versus* secondary catalytic cycles. Since protein substrate binding cannot be rate-limiting in the first catalytic cycle due to our experimental design, we favor an interpretation wherein the rate of YME1L protein unfolding in secondary catalytic cycles (k_2) is limited by protein substrate binding or a related kinetic step.

Examination of the rate constant data shown in Fig. 4C indicates that all rate constants related to YME1L catalyzed unfolding of SsrA-$Kaede_{Red}$ are estimated to be nearly independent of [H_2O_2]. The mean values of k_1 and k_2 estimated across all [H_2O_2] examined here are 0.32 ± 0.01 and 0.023 ± 0.006 s^{-1}, respectively. We note that conditions including 20–30 mM H_2O_2 reproducibly yield values for k_1 that are reduced by ~41% relative to conditions either lacking H_2O_2 or [H_2O_2] ≥ 50 mM H_2O_2. In contrast, we are unable to demonstrate any statistically significant relationship between k_2 and [H_2O_2]. As described above, k_1 must correspond to a kinetic step that occurs after the initial protein substrate binding step, which may include ATP binding, ATP hydrolysis, or protein unfolding. Therefore, Fig. 4C indicates that intermediate [H_2O_2] may promote decreased apparent rate constants related to nucleotide-dependent kinetic steps such as those mentioned above.

Nucleotide binding by YME1L is impacted by H_2O_2

The data presented above indicate that YME1L adopts specific conformational states that depend on the presence of nucleotide and/or oxidative stress. Furthermore, the impact of oxidative stress on YME1L catalyzed protein unfolding appears to be limited to low [H_2O_2] where a decrease in the apparent unfolding rate constant is observed. Based on these observations, we asked: does H_2O_2 impact either

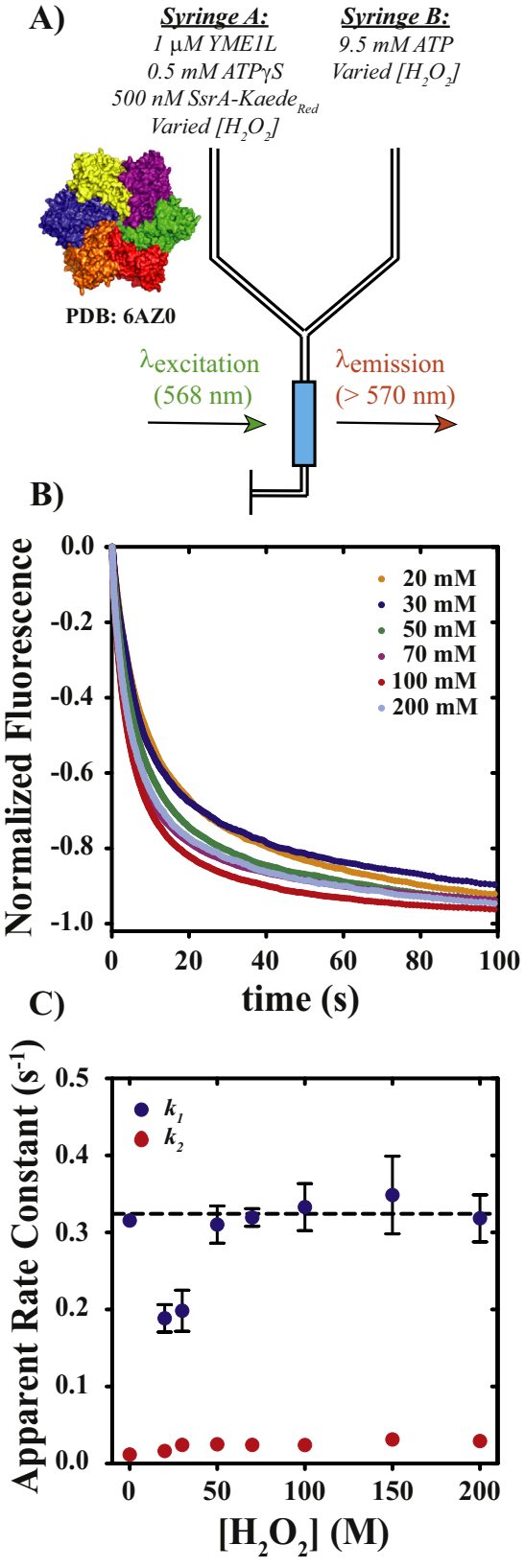

the rates of nucleotide association/dissociation or the overall nucleotide binding affinity? To investigate these questions, we applied a fluorescence resonance energy transfer-based method wherein YME1L was incubated in the presence of increasing concentrations of MANT-ATP. When excited at 295 nm, efficient energy transfer is known to occur between MANT-ATP and nearby tryptophan residues, thus allowing for straightforward measurements reporting on nucleotide binding [36–40]. However, initial titrations of YME1L with MANT-ATP under conditions of systematically varied [H_2O_2] revealed the impact of H_2O_2-associated tryptophan quenching on corresponding MANT-ATP emissions. Figure 5A illustrates a decrease in apparent emissions when YME1L is incubated with MANT-ATP under conditions of increasing [H_2O_2]. Regardless of [MANT-ATP], we observe an ~20% decrease in baseline corrected amplitude at 445 nm when [H_2O_2] is increased from 0 to 200 mM. Given that YME1L was incubated with MANT-ATP and H_2O_2 for 30 min prior to collection of emissions spectra, we expect that the [H_2O_2]-dependent decrease in baseline corrected emissions can be corrected by normalization of all data against a standard condition. Figure 5B depicts an overlay of such normalized data, where emissions spectra derived from conditions including 0.5 μM YME1L and varied [MANT-ATP] have been corrected using the 80 μM MANT-ATP condition as a reference. Using this strategy, we observe consistent amplitudes at 445 nm across varied [H_2O_2], which indicates a common baseline that is independent of hydrogen peroxide concentration (Fig. 5C–F).

Using this methodology, we performed a series of experiments where YME1L was rapidly mixed with varied concentrations of MANT-ATP and emissions were recorded as a function of increasing time.

Fig. 4. (A) Schematic representation of preincubation stopped-flow unfolding experiments. Syringe A contains the indicated reagents, YME1L, ATPγS, SsrA-Kaede$_{Red}$, and varied hydrogen peroxide concentrations (indicated in text). Syringe B contains ATP to initiate protein unfolding as well as H_2O_2. The hydrogen peroxide concentration is identical in Syringes A and B for an individual experiment. The contents of the two syringes are rapidly mixed in the stopped-flow spectrophotometer and SsrA-Kaede$_{Red}$ is excited at λ_{ex} = 568 nm. Emissions are observed above 570 nm with a 570-nm-long pass filter. (B) Fluorescence time courses for YME1L catalyzed SsrA-Kaede$_{Red}$ unfolding. Time courses represent 1 mM YME1L, 0.5 mM ATPγS, and 500 nM SsrA-Kaede$_{Red}$ preassembled prior to rapid mixing with 9.5 mM ATP in the presence of varied [H_2O_2]. Representative time courses are shown for [H_2O_2] ranging from 0 to 200 mM. (C) Mean values of k_1 and k_2 are estimated from NLLS analysis across all [H_2O_2] examined here as 0.32 ± 0.01 and 0.023 ± 0.006 s^{-1}, respectively. All data represent average values determined from at least three independent experiments. Error bars indicate ± standard deviation.

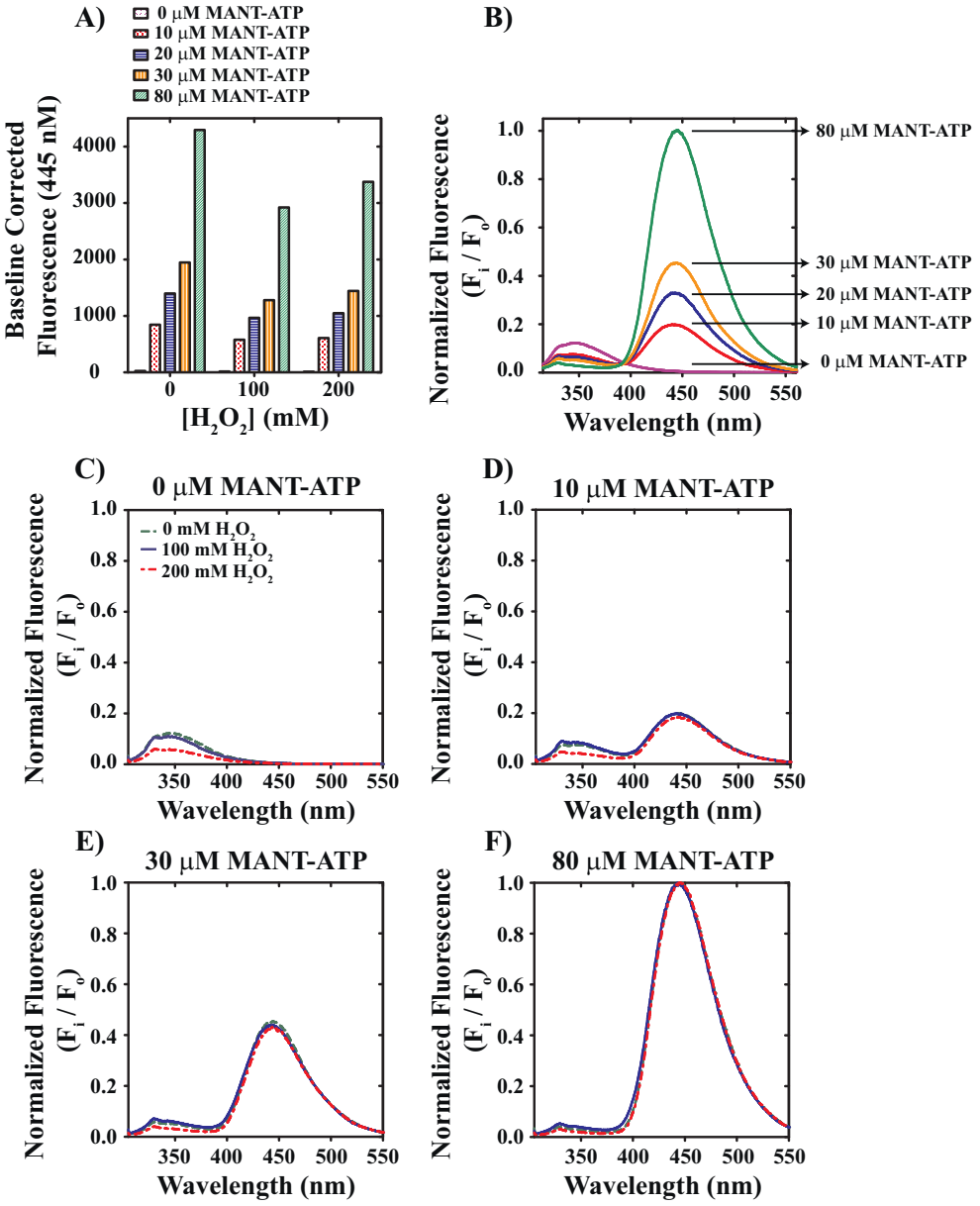

Fig. 5. Normalized MANT-ATP emissions are uniformly impacted by H_2O_2. (A) Baseline corrected MANT-ATP emissions at 445 nm exhibit a decrease in apparent amplitude in the presence *versus* absence of H_2O_2. Linear least squares analysis indicates that baseline corrected fluorescence at 445 nm is linearly dependent on [H_2O_2] with slopes of 49 ± 1, 33.2 ± 0.6, and 39.2 ± 0.5 AU/mM for conditions including 0, 100, and 200 mM H_2O_2, respectively. (B) Normalization of all spectra collected in the presence of a given [H_2O_2] to a common reference condition corrects for the ~20% quenching of tryptophan-dependent MANT-ATP emissions observed in panel A. Each fluorescence spectrum is labeled to indicate the corresponding [MANT-ATP]. (C–F) Normalization of emissions spectra collected in the presence of 0, 100, or 200 mM H_2O_2 to corresponding spectra collected with 80 mM MANT-ATP. Emissions spectra collected in the presence of 0, 100, or 200 mM H_2O_2 are represented as green broken lines, blue solid lines, or red dashed lines, respectively. All emissions spectra were collected by directly exciting tryptophan residues at λ_{ex} = 295 nm.

Representative time courses shown in Fig. 6A qualitatively indicate that the rate of nucleotide binding is dependent on both [nucleotide] and [H_2O_2]. All time courses are observed to exhibit biphasic kinetics, consistent with two distinct molecular events. Each time course was best described by a double-exponential function, thereby yielding estimates of the apparent first-order rate constants associated with each phase. From a plot of rate constant *versus* [MANT-ATP] (Fig. 6B), the association and dissociation rate constants can be determined from the slope and y-intercept, respectively [36,39]. We applied this

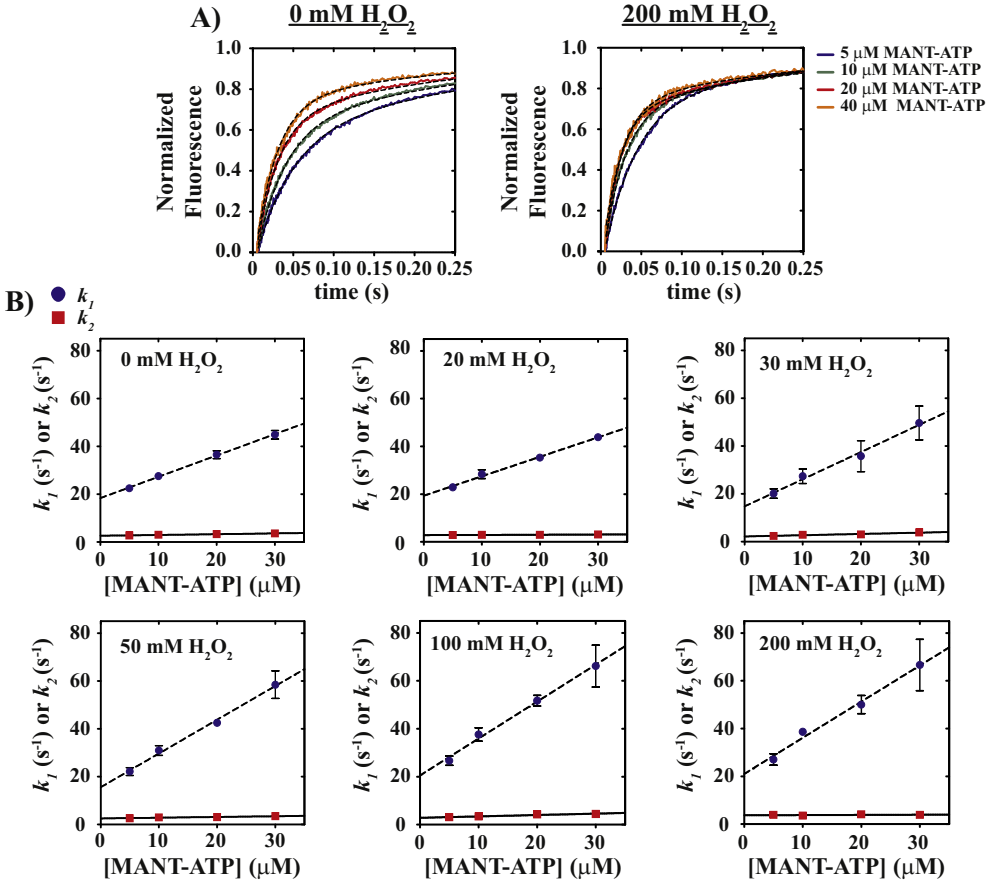

Fig. 6. (A) Fluorescence time courses for YME1L binding of MANT-ATP. Independent solutions containing [MANT-ATP] = 0–60 μM and 1 μM YME1L were rapidly mixed in a stopped-flow spectrophotometer. Signal is derived based on energy transfer between YME1L tryptophan residues and MANT-ATP with λ_{ex} = 295 nm. Emissions are observed above 400 nm with a 400-nm-long pass filter. The black dashed lines represent NLLS fits to a double-exponential function, Signal = $A_1 \cdot (1 - e^{-k_1 \cdot t}) + A_2 \cdot (1 - e^{-k_2 \cdot t})$, where A_x and k_x are apparent amplitude and rate constant terms. (B) MANT-ATP concentration dependence of the apparent rate constants k_1 and k_2 observed at varied [H_2O_2] = 0, 20, 30, 50, 100, and 200 mM. All data represent average values determined from at least three independent experiments. Error bars indicate ± standard deviation. Apparent rate constants are summarized in Table S2.

strategy across a varied range of [H_2O_2] such that the impact of oxidative stress on ATP binding could clearly be understood. For each condition, linear least squared analysis yields estimates of bimolecular association rate constants, $k_{a,1}$ and $k_{a,2}$, and first-order dissociation rate constants, $k_{d,1}$ and $k_{d,2}$, which represent parameters associated with each observed kinetic phase.

Figure 7A reveals that the association rate constant, $k_{a,1}$, describing MANT-ATP binding by YME1L is allosterically stimulated by increasing [H_2O_2] such that nucleotide is bound nearly 2-fold faster for conditions including 200 *versus* 0 mM H_2O_2. An NLLS fit with Eq. (3) of the plot of $k_{a,1}$ *versus* [H_2O_2] shown in Fig. 7A estimates a K_D = 32.4 ± 0.2 mM and a Hill Coefficient equal to 6 ± 3. Thus, multiple H_2O_2 molecules interact with YME1L under oxidative stress conditions such that the association rate constant describing ATP binding is stimulated. In contrast, no significant dependence on [H_2O_2] is observed for $k_{a,2}$. The apparent MANT-ATP dissociation rate constant, $k_{d,1}$, is only impacted under conditions including H_2O_2 between 30 and 50 mM (Fig. 7B), where an approximately 25% decrease in dissociation rate constant is observed. Similar to Fig. 7A, no significant dependence on [H_2O_2] is observed for $k_{d,2}$.

Time courses reporting on MANT-ATP binding to YME1L collected under any condition reported here display biphasic kinetics that correspond to distinct fast and slow phases. Thus, YME1L binding of nucleotide may occur via two distinct modes that correspond to high and low affinity binding states. Taking the ratio of dissociation and association rate

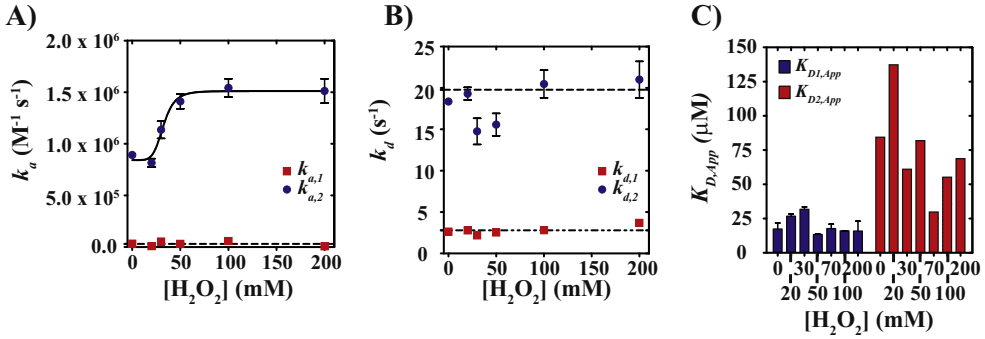

Fig. 7. (A) Dependence of apparent association rate constants describing YME1L binding of MANT-ATP on [H_2O_2]. Apparent rate constants for $k_{a,1}$ and $k_{a,2}$ are represented as blue spheres and red squares, respectively. The continuous solid line is the result of an NLLS fit to Eq. (2) where the affinity and Hill coefficient are estimated as K_D = 32.4 ± 0.2 mM and n = 6 ± 3. The apparent association rate constants estimated in the absence of H_2O_2 or in the presence of saturating [H_2O_2] are (8.4 ± 0.7) × 10^5 and (1.5 ± 0.9) × 10^6 M^{-1} s^{-1}, respectively. No significant dependence on [H_2O_2] is observed for $k_{a,2}$, where the mean value across all conditions examined here equals (4 ± 2) × 10^4 M^{-1} s^{-1}. (B) Dependence on [H_2O_2] of apparent rate constants describing MANT-ATP dissociation from YME1L. Apparent rate constants for $k_{d,1}$ and $k_{d,2}$ are represented as blue spheres and red squares, respectively. No significant dependence on [H_2O_2] is observed for either $k_{d,1}$ and $k_{d,2}$ such that the mean values of either parameter are estimated as 2.8 ± 0.5 and 20 ± 1 s^{-1}, respectively, for all conditions except 30 and 50 mM H_2O_2, where the mean $k_{d,1}$ is decreased to 15.2 ± 0.6 s^{-1}. (C) Dependence of apparent dissociation equilibrium constant for YME1L binding of MANT-ATP on [H_2O_2]. $K_{D,1}$ and $K_{D,2}$ are observed to fluctuate about mean values equal to 20 ± 7 and 74 ± 33 μM, respectively. All data represent average values determined from at least three independent experiments. Error bars indicate ± standard deviation.

constant data allows for an estimation of equilibrium binding affinity separately for both of these kinetic events. Figure 7C displays the result of these calculations where no significant dependence in dissociation equilibrium constant on [H_2O_2] is observed for either the fast- ($K_{D,1}$) or slow-phase ($K_{D,2}$). $K_{D,1}$ and $K_{D,2}$ are observed to fluctuate about mean values equal to 20 ± 7 and 74 ± 33 μM, respectively. These data indicate that the high-affinity YME1L mode binds ATP first, followed next by slower binding with a lower affinity. As such, oxidative conditions that yield depletion of the mitochondrial ATP pool may yield conditions of intermediate [ATP] that promote YME1L complexes preferentially subsaturated with ATP as reflected in the negatively cooperative binding constants. This negative cooperativity is not observed to significantly depend on [H_2O_2] under any condition examined here where the mean ratio of $K_{D,2}$ to $K_{D,1}$ is 3.9 ± 1.7. Positive values that deviate from unity for the ratio of $K_{D,2}$ to $K_{D,1}$ suggest that ligand binding is negatively cooperative.

A secondary explanation for the observation of biphasic kinetics is a slow conformational change that occurs upon nucleotide binding. Any signal changes associated with the binding of MANT-ATP to YME1L would be attributed to energy transfer between nearby tryptophan residues and MANT-ATP. A piece of evidence that disputes a conformational change mechanism is the observation that the association rate constant for the second phase, $k_{a,2}$, is independent of [H_2O_2], whereas $k_{a,1}$ displays a sigmoidal dependence on hydrogen peroxide concentration. If the second phase represents a kinetic step that immediately follows nucleotide binding, then that step will be kinetically coupled to nucleotide binding. Consequently, this would require that $k_{a,2}$ exhibit a hydrogen peroxide concentration dependence as observed for $k_{a,1}$. Given these data, we favor a model wherein the second phase represents a second nucleotide binding event that occurs with negative cooperativity.

Discussion

Inner-membrane proteases such as YME1L and OMA1 are critical to the maintenance of proteostasis in the intermembrane space as well as regulation of mitochondrial morphology. Until recently, *in vitro* studies of mitochondrial inner membrane proteases were hindered by a lack of available methodology leading to the production of quantities of soluble protein useable in biochemical studies. However, Shi and coworkers [20] recently reported the first methodology to overexpress and purifiy soluble YME1L assembled into the appropriate hexameric state. This methodology involved expression of the soluble YME1L domains (AAA+ ATPase and M41 zinc-metalloprotease domains) fused at the N-terminus to a short polypeptide (cc-Hex) known to form hexamers [21]. In the absence of this fusion, the soluble YME1L domains appear to remain monomeric, a state inconsistent with the active hexameric form for YME1L and most AAA+ ATPases [41–48]. This strategy was also employed to develop a

soluble variant of the mitochondrial AFG3L2 protease, which contrasts YME1L through projection of soluble catalytic domains into the matrix compartment [49]. The successful reconstitution of protease complexes previously resistant to recombinant overexpression and isolation such as YME1L and AFG3L2 has significantly advanced our ability to investigate the biochemical details underlying inner-membrane protease function.

YME1L conformation is dependent on solution conditions

Using the methodology reported by Shi and coworkers [20], we have demonstrated YME1L to be conformationally dynamic under oxidative stress conditions. Our data support two unique driving forces for YME1L conformational changes under the conditions examined here: (1) [H_2O_2] and (2) [nucleotide]. Limited proteolysis experiments strongly indicate that YME1L adopts two distinct conformational states when nucleotide is absent that depend on oxidative stress. Those results demonstrate increased YME1L sensitivity to proteinase K-dependent digestion under oxidative conditions relative to non-oxidative conditions. Figure 1A–B highlights that the YME1L conformation observed under oxidative stress in the absence of nucleotide is unique relative to either non-stress conditions or any condition with nucleotide present. Moreover, complementary tryptophan quenching experiments suggest that this involves the interaction of 1 H_2O_2 molecule per YME1L monomer with an affinity equal to ~30 mM. The introduction of nucleotide promotes states unique from the apo, stress-induced conformation that are generally described as apo-like (non-stress), nucleotide-subsaturated, or nucleotide-saturated. Given that YME1L is a substrate for OMA1 under stress conditions with significant ATP depletion [17,19], our data suggest that oxidative stress combined with significant ATP depletion may promote a YME1L conformational change that results in exposure of OMA1-recongition sites not previously accessible under non-stress conditions.

Nucleotide binding kinetics

By considering pre-steady-state nucleotide binding data alongside available steady-state ATP hydrolysis data, valuable predictions can be made regarding the molecular mechanism describing a cycle of ATP binding and hydrolysis. Pre-steady-state kinetic data reporting on MANT-ATP binding under non-oxidative conditions yield estimates of the association and dissociation rate constants equal to $8.92 \times 10^5\ M^{-1}\ s^{-1}$ and $18.36\ s^{-1}$, respectively. The ratio of these values suggests an apparent K_D for high-affinity nucleotide binding under non-oxidative conditions equal to 20.6 μM. This contrasts the Michaelis constant, K_M, recently reported as 1.4 mM, and represents an approximately 70-fold difference in numerical value between the apparent K_D and K_M [20]. However, discrepancies between the dissociation equilibrium and Michaelis constants have precedent with one example being *Escherichia coli* ClpA catalyzed hydrolysis of ATPγS, where the K_M = 134 μM and K_D = 6.2 μM (21-fold difference) [50]. Steady-state kinetic analysis using the Michaelis Menten mechanism,

$$E + S \underset{k_{-1}}{\overset{k_1}{\rightleftarrows}} ES \xrightarrow{k_2} E + P$$

assumes a rapid-equilibrium where the rate of ES complex dissociation, k_{-1}, is much larger than the turnover number, k_2. Given that

$$K_M = \frac{k_{-1} + k_2}{k_1} \quad (1)$$

K_M cannot equal the dissociation equilibrium constant ($K_D = \frac{k_{-1}}{k_1}$) if the rapid-equilibrium assumption is not satisfied, where $k_{-1} >> k_2$. That is, the kinetic step following ATP binding must be small relative to the rate constant describing nucleotide dissociation. To estimate k_2, we input known values for the K_M, k_{-1}, and k_1 determined here and elsewhere [20] into Eq. (1) shown above and solved for k_2. From this, we estimate k_2 to equal $1.23 \times 10^3\ s^{-1}$, which is considerably faster than the reported value. However, we expect that this is a consequence of intermediate kinetic steps that may occur between nucleotide binding and hydrolysis events. Further pre-steady-state analysis will be necessary to elucidate the complete molecular mechanism describing YME1L catalyzed ATP binding and hydrolysis.

YME1L conformational dynamics may support OMA1 resistance

The YME1L conformational states reported here depend on solution conditions that include both oxidative stress and nucleotide concentration. Moreover, these conformational shifts induce changes to the behavior of the enzyme with examples that include [H_2O_2]-dependent stimulation of nucleotide binding as well as subtle decreases in the rate constants describing nucleotide dissociation and protein substrate unfolding. Our data suggest that multiple H_2O_2 molecules interact per YME1L hexamer thereby influencing the physical behavior of the enzyme. The data shown in Fig. 7A strongly implicate hydrogen peroxide as an allosteric activator of ATP binding. In fact, oxidative treatment followed by extensive dialysis suggests that the allosteric effects of H_2O_2 on YME1L may be reversible (Fig. 1D), which would necessarily involve non-covalent protein:H_2O_2 interactions. However, it

is unclear whether this is a specific and reversible protein–ligand interaction, the consequence of ROS-associated oxidation events at allosteric sites, or both. Irreversible events may involve the oxidation of lysine [25], arginine [23,51], histidine [24], or cysteine [22,52] residues, where post-translational modifications to any of these amino acids necessarily alter the charge state under physiological conditions. For example, H_2O_2-dependent oxidation of L-arginine can yield L-citrulline as a product, which converts the positive charge associated with a side-chain guanidinium to a neutral charge associated with the citrulline ureido functional group [23,51]. A similar example is found in cysteine oxidation, where sulfhydryl oxidation to sulfenic, sulfinic, and sulfonic acids can occur, thus introducing negative charge at previously neutral residue positions [22]. Alterations in the charge of a single-residue position can also influence the pK_a of neighboring amino acid residues. Therefore, post-translational oxidation events may lead to conformational changes that compensate for altered charge distribution.

The oxidation of common amino acids to alternate forms can occur via reversible or irreversible reaction pathways to facilitate function as redox-sensors or redox-switches. Reversible events include the formation of disulfide bonds or *S*-glutathionylation. These modifications represent mechanisms that may allow for the monitoring of cellular redox state such that elevated ROS may regulate protein function for a range of applications that can include oxidative protection or cellular signaling. One example of reversible redox regulation is that of plant chloroplast ATP synthase, which involves a regulatory disulfide bond that impacts ATP synthesis [22]. In contrast, higher cysteine oxidation states such as the sulfinic (SO_2H) and sulfonic (SO_3H) acid forms represent largely irreversible oxidation events that are primarily associated with significantly elevated concentrations of ROS. Given that the hydrogen peroxide concentrations utilized here likely exceed physiological concentrations, oxidation of many YME1L residues occurring here may be irreversible. However, given observed reversibility in YME1L conformation by limited proteolysis methods, we do not expect all protein:ROS interactions to be irreversible. In addition, the estimated affinity between YME1L and H_2O_2 is approximately 30 mM. Although yeast can tolerate acute oxidative treatments that include [H_2O_2] greater than 30 mM, we do not expect cellular hydrogen peroxide to elevate beyond micromolar concentrations normally. From this, we do not expect the entire YME1L population to behave *in vivo* as observed here, but instead propose that a subset of enzyme would be influenced, whether by reversible or irreversible oxidations, or both, to stabilize the conformational state(s) observed here.

The conformational distribution observed here may suggest a mechanism wherein oxidative stress and nucleotide ligation state promote a YME1L state that is recognizable by OMA1 as a substrate. Negatively cooperative nucleotide binding is observed under all conditions examined here, where affinities are estimated as 20 ± 7 and 74 ± 33 μM. Moreover, our limited proteolysis experiments reveal distinct YME1L conformational states for oxidative conditions that include [ATPγS] = 0.25 *versus* conditions lacking nucleotide. Based on these observations, the distribution of YME1L conformational states that populate under oxidative conditions should represent a continuum when nucleotide concentrations decrease in living systems. That is to say, as ATP depletion occurs during oxidative stress, intermediate conditions are expected that would preferentially populate a nucleotide-subsaturated YME1L complex. Such conditions may favor increased ATP binding by YME1L with concomitant decreases in nucleotide dissociation that contribute to stabilization of a specific conformational state. However, it is unclear whether the apo-state and nucleotide-subsaturated YME1L complex could both serve as substrates for OMA1 under oxidative conditions. One hypothesis is that nucleotide-subsaturated YME1L complexes adopt a conformation that is resistant to OMA1 degradation under oxidative stress such that a reserve population of protease is available for the time at which the stress is resolved. The observation of a decreased apparent rate constant for YME1L-catalyzed protein unfolding in the presence of specific hydrogen peroxide concentrations is consistent with this model. Despite this, additional work is warranted to fully elucidate the connection between YME1L conformation and *in vivo* function.

Materials and Methods

Materials

All solutions were prepared with reagent-grade chemicals in double-distilled water produced from a Purelab Ultra Genetic System (Siemens Water Technology). MANT-ATP was prepared as described previously and purified using reverse-phase chromatography [53]. Product MANT-ATP was characterized by thin layer chromatography and by mass spectrometry. MANT-ATP and ATP/ATPγS concentrations were determined spectrophotometrically using extinction coefficients $\varepsilon_{255} = 2.33 \times 10^4\ M^{-1}\ cm^{-1}$ and $\varepsilon_{260} = 1.54 \times 10^4\ M^{-1}\ cm^{-1}$, respectively. All genes were synthesized and each cloned into the pET-24a (+) vector commercially by Genscript (Piscataway, NJ, USA). The hexYME1L gene was designed as previously described with the addition of an N-terminal His_6-SUMO tag [20]. Briefly, the hexYME1L construct represents a YME1L truncation where the insoluble

transmembrane YME1L segment has been replaced with the de novo designed cc-hex peptide sequence [21]. The hexYME1L gene product assembles into hexamers as a consequence of the self-assembly properties of the cc-hex sequence, thereby yielding the enzymatically active YME1L oligomer. SsrA-Kaede$_{Red}$ was overexpressed and purified as previously described [35].

Protein expression and purification

YME1L (hexYME1L) was prepared as an N-terminal His$_6$-SUMO fusion and overexpressed from the pET-24a(+) vector in BL21(DE3) competent cells. Bacterial cultures were initially grown in Lysogeny broth (LB) at 37 °C, followed by induction at OD_{600} = 0.6 absorbance units with 0.5 mM IPTG (ThermoFisher Scientific, Waltham, MA, USA) and incubation with shaking at 18 °C for 16 h. The harvested cell paste was resuspended in chilled lysis buffer containing 25 mM Tris (pH 8.3), 500 mM NaCl, 20% glycerol, 10 mM 2-mercaptoethanol, 10 mM imidazole (pH 8), 0.05% v/v Tween-80, 0.1 mM EDTA, and 1 mM PMSF. The resulting suspension was subjected to sonication and clarified by centrifugation at ~50, 000*g*. Affinity chromatography was next applied such that the supernatant resulting from the previous centrifugation step was incubated at 4 °C for 2 h with Ni-nitriloacetic acid solid-phase resin (Ni-NTA, G-Biosciences, St. Louis, MO, USA) previously equilibrated with lysis buffer. Following incubation, the Ni-NTA resin was subjected to centrifugation at ~250*g* to isolate solid-phase resin. The supernatant was discarded and the Ni-NTA resin washed with fresh lysis buffer. All His$_6$-SUMO-fusion proteins were dissociated from the resin by gravity flow using elution buffer containing 25 mM Tris (pH 8.3), 500 mM NaCl, 20% glycerol, 10 mM 2-mercaptoethanol, 250 mM imidazole (pH 8), and 0.05% v/v Tween-80. The His$_6$-SUMO tag was removed from all fusion proteins by overnight digestion with His$_6$-tagged Ulp1 protease [54]. Cleaved protein was separated from His$_6$-Ulp1 and uncleaved protein by additional Ni-NTA binding. The resulting YME1L was flash-frozen in liquid nitrogen, and stored at −80 °C. Prior to storage, purity was judged to be >95% by Coomassie staining. Protein concentration was determined spectrophotometrically in reaction buffer H150 using an extinction coefficient $\varepsilon_{280} = 3.29 \times 10^4\ M^{-1}\ cm^{-1}$.

Methods

Tryptophan quenching experiments

All fluorescence measurements were collected with a Hitachi F-4500 fluorescence spectrophotometer. Samples were excited at 295 nm and emissions recorded from 305 to 400 nm. Two samples were prepared, each containing 1 μM YME1L in H150 reaction buffer [25 mM Hepes (pH 7.5) at 25 °C, 150 mM NaCl, 10% glycerol, 2 mM 2-mercaptoethanol, 10 mM $MgCl_2$, and 0.5 mM $ZnCl_2$] in the presence and absence of 1.4 mM ATPγS. After incubating for 30 min in the spectrophotometer, both samples were titrated with H_2O_2 (stock concentration of 0.979 M) to achieve a range of H_2O_2 concentrations from 0 to 200 mM. Following each titrant addition, samples were incubated again for 10 min and emissions spectra collected.

The H_2O_2 concentration dependences of YME1L tryptophan emissions displayed in Fig. 3A–B were subjected to NLLS analysis using the infinitely cooperative or Hill model given by Eq. (2):

$$S_{obs} = \frac{A_{max}(K_a[H_2O_2])^{n_H}}{1 + (K_a[H_2O_2])^{n_H}} + b \qquad (2)$$

where S_{obs} is the observed fluorescence signal, A_{max} is the maximum apparent amplitude, K_a is the association equilibrium constant, n is the Hill coefficient, and b is the y-intercept.

Limited proteolysis assays

Limited proteolysis experiments were carried out in H150 reaction buffer [25 mM Hepes (pH 7.5) at 25 °C, 150 mM NaCl, 10% glycerol, 2 mM 2-mercaptoethanol, 10 mM $MgCl_2$, and 0.5 mM $ZnCl_2$]. YME1L (3 μM) was incubated for 1 h with 25 nM proteinase K and varying concentrations of H_2O_2 (0 and 200 H_2O_2) and ATPγS (0, 0.25, 0.5, 1.4, and 3 mM ATPγS). Samples were collected at 10-min time intervals and quenched with SDS sample-loading buffer [250 mM Tris HCl (pH 6.8), 8% w/v SDS, 0.1% w/v bromophenol blue, 40% v/v glycerol, and 200 mM 2-mercaptoethanol] supplemented with 10 mM PMSF before boiling at 100 °C for 10 min to insure denaturation. Separation of digestion products was performed with SDS-PAGE gel electrophoresis and digestion products were visualized by coomassie staining.

Pre-steady-state kinetic analysis

All stopped-flow fluorescence experiments were performed using an Applied Photophysics SX.20 stopped-flow fluorometer (Letherhead, UK). All reactions were performed at 25 °C in buffer H150 [25 mM Hepes (pH 7.5) at 25 °C, 150 mM NaCl, 10% glycerol, 2 mM 2-mercaptoethanol, 10 mM $MgCl_2$, and 0.5 mM $ZnCl_2$]. For protein unfolding experiments, the following solution conditions were used. Syringe A contained 1 μM YME1L, 0.5 mM ATPγS, 500 nM SsrA-Kaede$_{Red}$, and varied concentrations of hydrogen peroxide. Syringe B contained 9.5 mM ATP and a concentration of H_2O_2

equal to that included in Syringe A. Experiments performed in the absence of ATP yield no observed protein unfolding and demonstrate a requirement for ATP to fuel YME1L catalyzed protein unfolding (Fig. S2). Final [H_2O_2] are indicated in the text. Both solutions were incubated for 50 min at 25 °C to allow complex formation to reach equilibrium. Prior to mixing, both solutions were incubated for an additional 10 min at 25 °C in the stopped-flow instrument to establish thermal equilibrium. Additional incubation of either solution had no effect on the observed fluorescence time courses. SsrA-Kaede$_{Red}$ was excited at λ_{ex} = 568 nm and fluorescence emissions were observed above 570 nm using a 570-nm-long pass filter. All kinetic traces shown represent the average of at least seven individual determinations. Averaged time courses were subjected to NLLS analysis using a double exponential function.

Nucleotide binding kinetics were observed based on energy transfer between YME1L tryptophan residues and MANT-ATP as described previously [36,37]. All experiments were performed in buffer H150 lacking $MgCl_2$ under pseudo-first order conditions with [MANT-ATP] in at least 10-fold excess of [YME1L]. Syringes A and B contained 1 μM YME1L and varied concentrations of MANT-ATP, respectively. Final [MANT-ATP] is described in text. Both syringes contained systematically varied [H_2O_2], and all final concentrations are indicated in text. YME1L tryptophan residues were excited at λ_{ex} = 295 nm, and fluorescence emissions were observed above 400 nm with a 400-nm-long-pass filter. The MANT-ATP emission maximum under these conditions was verified by steady-state fluorescence titrations of YME1L with MANT-ATP as described in text. All kinetic traces shown represent the average of at least seven individual determinations. Averaged time courses were subjected to NLLS analysis using a double exponential function.

The H_2O_2 concentration dependence of the rate constant describing MANT-ATP association with YME1L displayed in Fig. 7A was subjected to NLLS analysis using the infinitely cooperative or Hill model given by Eq. (3):

$$k_a = \frac{k_{a,max}(K_a[H_2O_2])^n}{1 + (K_a[H_2O_2])^n} + b \qquad (3)$$

where k_a is the apparent association rate constant, $k_{a,max}$ is the maximum apparent association rate constant, K_a is the association equilibrium constant, n is the Hill coefficient, and b is the y-intercept.

Yeast viability assay

S. cerevisiae knockout strains for YME1, OMA1, and MGM1 (YPR024W, YKR087C, and YOR211C, respectively) were obtained from the Dharmacon yeast knockout collection (Lafayette, CO). Wild-type yeast were kindly provided by James Robertson of the Department of Biology at Middle Tennessee State University. Yeasts were grown in YPD media (Fisher Scientific, Pittsburgh, PA) to both mid-logarithmic and stationary phases. Cell phase was confirmed by optical density measurement (OD_{600} = 0.5 for mid-logarithmic cells and OD_{600} = 1 or higher for stationary phase). To insure consistency, stationary phase cells were diluted with YPD media until an absorbance of OD_{600} = 0.5 was observed. Samples were collected in 1-mL volumes, and cells were washed twice with 0.1 M Hepes (pH 7.5). Cells were resuspended in 1 mL of 0.1 M Hepes (pH 7.5) and varying concentrations of H_2O_2 (0, 10, 20, 30, and 40 mM) and incubated for 1 h at 30 °C. Following incubation, cells were again washed twice by centrifugation and resuspended in 0.1 M Hepes (pH 7.5) buffer solution. Each condition (3 μL) was spotted on YPD agar plates and incubated at 30 °C for 2–3 days.

Supplementary data to this article can be found online at https://doi.org/10.1016/j.jmb.2019.01.039.

Acknowledgments

We thank TJ Lamantia and Jessica Rodriguez for critical discussions and comments on this manuscript. We are also indebted to Donald A. Burden for preparation of MANT-ATP as previously described. This work was supported in part by funding to JMM from a generous startup package from Middle Tennessee State University (MTSU) and from the MTSU Molecular Biosciences (MOBI) doctoral program. C.B. received financial support from the MTSU Molecular Biosciences doctoral program. J.D.M. received financial support from the MTSU Department of Chemistry M.S. degree program.

Conflicts of Interest: The authors declare no conflicts of interest related to any work reported here.

Received 18 December 2018;
Received in revised form 11 January 2019;
Accepted 27 January 2019
Available online 5 February 2019

Keywords:
YME1;
mitochondria;
AAA+ protease;
zinc-metalloprotease;
reactive oxygen species

Abbreviations used:
NTP, nucleoside triphosphate; ATP, adenosine triphosphate; AAA+, ATPases Associated with various cellular Activities;

YME1, yeast mitochondrial escape protein 1; IMM, inner mitochondrial membrane; NLLS, nonlinear least squares; ROS, reactive oxygen species.

References

[1] R.M. Levytskyy, I. Bohovych, O. Khalimonchuk, Metalloproteases of the inner mitochondrial membrane, Biochemistry 56 (2017) 4737–4746, https://doi.org/10.1021/acs.biochem.7b00663.

[2] D.C. Chan, Mitochondria: dynamic organelles in disease, aging, and development, Cell 125 (2006) 1241–1252, https://doi.org/10.1016/j.cell.2006.06.010.

[3] M.P. Murphy, How mitochondria produce reactive oxygen species, Biochem. J. 417 (2009) 1–13, https://doi.org/10.1042/BJ20081386.

[4] J.F. Turrens, Mitochondrial formation of reactive oxygen species, J. Physiol. 552 (2003) 335–344, https://doi.org/10.1113/jphysiol.2003.049478.

[5] L.A. Sena, N.S. Chandel, Physiological roles of mitochondrial reactive oxygen species, Mol. Cell 48 (2012) 158–167, https://doi.org/10.1016/j.molcel.2012.09.025.

[6] P. Dromparis, E.D. Michelakis, Mitochondria in vascular health and disease, Annu. Rev. Physiol. 75 (2013) 95–126, https://doi.org/10.1146/annurev-physiol-030212-183804.

[7] A.T. Akhmedov, V. Rybin, J. Marin-Garcia, Mitochondrial oxidative metabolism and uncoupling proteins in the failing heart, Heart Fail. Rev. 20 (2015) 227–249, https://doi.org/10.1007/s10741-014-9457-4.

[8] M.D. Brand, Uncoupling to survive? The role of mitochondrial inefficiency in ageing, Exp. Gerontol. 35 (2000) 811–820.

[9] D.A. Brown, et al., Expert consensus document: mitochondrial function as a therapeutic target in heart failure, Nat. Rev. Cardiol. 14 (2017) 238–250, https://doi.org/10.1038/nrcardio.2016.203.

[10] S.M. Rafelski, Mitochondrial network morphology: building an integrative, geometrical view, BMC Biol. 11 (2013) 71, https://doi.org/10.1186/1741-7007-11-71.

[11] T. Ban, et al., Molecular basis of selective mitochondrial fusion by heterotypic action between OPA1 and cardiolipin, Nat. Cell Biol. 19 (2017) 856–863, https://doi.org/10.1038/ncb3560.

[12] R. Liu, D.C. Chan, OPA1 and cardiolipin team up for mitochondrial fusion, Nat. Cell Biol. 19 (2017) 760–762, https://doi.org/10.1038/ncb3565.

[13] A.M. van der Bliek, Q. Shen, S. Kawajiri, Mechanisms of mitochondrial fission and fusion, Cold Spring Harb. Perspect. Biol. 5 (2013)https://doi.org/10.1101/cshperspect.a011072.

[14] R.J. Youle, A.M. van der Bliek, Mitochondrial fission, fusion, and stress, Science 337 (2012) 1062–1065, https://doi.org/10.1126/science.1219855.

[15] V. Del Dotto, M. Fogazza, V. Carelli, M. Rugolo, C. Zanna, Eight human OPA1 isoforms, long and short: what are they for? Biochim. Biophys. Acta Bioenerg. 1859 (2018) 263–269, https://doi.org/10.1016/j.bbabio.2018.01.005.

[16] T. Wai, et al., Imbalanced OPA1 processing and mitochondrial fragmentation cause heart failure in mice, Science 350 (2015), aad0116. https://doi.org/10.1126/science.aad0116.

[17] T.K. Rainbolt, J. Lebeau, C. Puchades, R.L. Wiseman, Reciprocal degradation of YME1L and OMA1 adapts mitochondrial proteolytic activity during stress, Cell Rep. 14 (2016) 2041–2049, https://doi.org/10.1016/j.celrep.2016.02.011.

[18] K. Zhang, H. Li, Z. Song, Membrane depolarization activates the mitochondrial protease OMA1 by stimulating self-cleavage, EMBO Rep. 15 (2014) 576–585, https://doi.org/10.1002/embr.201338240.

[19] T.K. Rainbolt, J.M. Saunders, R.L. Wiseman, YME1L degradation reduces mitochondrial proteolytic capacity during oxidative stress, EMBO Rep. 16 (2015) 97–106, https://doi.org/10.15252/embr.201438976.

[20] H. Shi, A.J. Rampello, S.E. Glynn, Engineered AAA+ proteases reveal principles of proteolysis at the mitochondrial inner membrane, Nat. Commun. 7 (2016) 13301, https://doi.org/10.1038/ncomms13301.

[21] N.R. Zaccai, et al., A de novo peptide hexamer with a mutable channel, Nat. Chem. Biol. 7 (2011) 935–941, https://doi.org/10.1038/nchembio.692.

[22] H.S. Chung, S.B. Wang, V. Venkatraman, C.I. Murray, J.E. Van Eyk, Cysteine oxidative posttranslational modifications: emerging regulation in the cardiovascular system, Circ. Res. 112 (2013) 382–392, https://doi.org/10.1161/CIRCRESAHA.112.268680.

[23] R.A. Pufahl, J.S. Wishnok, M.A. Marletta, Hydrogen peroxide-supported oxidation of NG-hydroxy-L-arginine by nitric oxide synthase, Biochemistry 34 (1995) 1930–1941.

[24] C. Schoneich, Mechanisms of metal-catalyzed oxidation of histidine to 2-oxo-histidine in peptides and proteins, J. Pharm. Biomed. Anal. 21 (2000) 1093–1097.

[25] M. Utrera, J.G. Rodriguez-Carpena, D. Morcuende, M. Estevez, Formation of lysine-derived oxidation products and loss of tryptophan during processing of porcine patties with added avocado byproducts, J. Agric. Food Chem. 60 (2012) 3917–3926, https://doi.org/10.1021/jf3001313.

[26] K. Arnold, L. Bordoli, J. Kopp, T. Schwede, The SWISS-MODEL workspace: a web-based environment for protein structure homology modelling, Bioinformatics 22 (2006) 195–201, https://doi.org/10.1093/bioinformatics/bti770.

[27] M. Biasini, et al., SWISS-MODEL: modelling protein tertiary and quaternary structure using evolutionary information, Nucleic Acids Res. 42 (2014) W252–W258, https://doi.org/10.1093/nar/gku340.

[28] S. Bienert, et al., The SWISS-MODEL Repository—new features and functionality, Nucleic Acids Res. 45 (2017) D313–D319, https://doi.org/10.1093/nar/gkw1132.

[29] N. Guex, M.C. Peitsch, T. Schwede, Automated comparative protein structure modeling with SWISS-MODEL and Swiss-PdbViewer: a historical perspective, Electrophoresis 30 (Suppl. 1) (2009) S162–S173, https://doi.org/10.1002/elps.200900140.

[30] F. Kiefer, K. Arnold, M. Kunzli, L. Bordoli, T. Schwede, The SWISS-MODEL repository and associated resources, Nucleic Acids Res. 37 (2009) D387–D392, https://doi.org/10.1093/nar/gkn750.

[31] P. Cavatorta, R. Favilla, A. Mazzini, Fluorescence quenching of tryptophan and related compounds by hydrogen peroxide, Biochim. Biophys. Acta 578 (1979) 541–546.

[32] J.R. Lakowicz, Principles of Fluorescence Spectroscopy, Springer, 2006.

[33] Z.H. Shah, et al., The human homologue of the yeast mitochondrial AAA metalloprotease Yme1p complements a yeast yme1 disruptant, FEBS Lett. 478 (2000) 267–270.

[34] S.E. Glynn, A.R. Nager, T.A. Baker, R.T. Sauer, Dynamic and static components power unfolding in topologically closed rings of a AAA+ proteolytic machine, Nat. Struct. Mol. Biol. 19 (2012) 616–622, https://doi.org/10.1038/nsmb.2288.

[35] J.D. Marsee, A. Ridings, T. Yu, J.M. Miller, *Mycobacterium tuberculosis* ClpC1 N-terminal domain is dispensible for

adaptor protein-dependent allosteric regulation, Int. J. Mol. Sci. 19 (2018) 3651.
[36] M.J. Bradley, E.M. De La Cruz, Analyzing ATP utilization by DEAD-box RNA helicases using kinetic and equilibrium methods, Methods Enzymol. 511 (2012) 29–63, https://doi.org/10.1016/B978-0-12-396546-2.00002-4.
[37] A. Henn, W. Cao, D.D. Hackney, E.M. De La Cruz, The ATPase cycle mechanism of the DEAD-box rRNA helicase, DbpA, J. Mol. Biol. 377 (2008) 193–205, https://doi.org/10.1016/j.jmb.2007.12.046.
[38] Y.J. Jeong, D.E. Kim, S.S. Patel, Nucleotide binding induces conformational changes in *Escherichia coli* transcription termination factor rho, J. Biol. Chem. 279 (2004) 18370–18376, https://doi.org/10.1074/jbc.M309162200.
[39] M.A. Talavera, E.M. De La Cruz, Equilibrium axand kinetic analysis of nucleotide binding to the DEAD-box RNA helicase DbpA, Biochemistry 44 (2005) 959–970, https://doi.org/10.1021/bi048253i.
[40] Y.C. Kim, A. Snoberger, J. Schupp, D.M. Smith, ATP binding to neighbouring subunits and intersubunit allosteric coupling underlie proteasomal ATPase function, Nat. Commun. 6 (2015) 8520, https://doi.org/10.1038/ncomms9520.
[41] C. Puchades, et al., Structure of the mitochondrial inner membrane AAA+ protease YME1 gives insight into substrate processing, Science 358 (2017), https://doi.org/10.1126/science.aao0464.
[42] J.M. Miller, E.J. Enemark, Fundamental characteristics of AAA+ protein family structure and function, Archaea 2016 (2016), 9294307. https://doi.org/10.1155/2016/9294307.
[43] J.P. Erzberger, J.M. Berger, Evolutionary relationships and structural mechanisms of AAA+ proteins, Annu. Rev. Biophys. Biomol. Struct. 35 (2006) 93–114, https://doi.org/10.1146/annurev.biophys.35.040405.101933.
[44] A.F. Neuwald, L. Aravind, J.L. Spouge, E.V. Koonin, AAA+: a class of chaperone-like ATPases associated with the assembly, operation, and disassembly of protein complexes, Genome Res. 9 (1999) 27–43.
[45] S.N. Gates, et al., Ratchet-like polypeptide translocation mechanism of the AAA+ disaggregase Hsp104, Science 357 (2017) 273–279, https://doi.org/10.1126/science.aan1052.
[46] J.M. Miller, B.T. Arachea, L.B. Epling, E.J. Enemark, Analysis of the crystal structure of an active MCM hexamer, elife 3 (2014), e03433. https://doi.org/10.7554/eLife.03433.
[47] E.J. Enemark, L. Joshua-Tor, Mechanism of DNA translocation in a replicative hexameric helicase, Nature 442 (2006) 270–275, https://doi.org/10.1038/nature04943.
[48] C. Bieniossek, B. Niederhauser, U.M. Baumann, The crystal structure of apo-FtsH reveals domain movements necessary for substrate unfolding and translocation, Proc. Natl. Acad. Sci. U. S. A. 106 (2009) 21579–21584, https://doi.org/10.1073/pnas.0910708106.
[49] B. Ding, D.W. Martin, A.J. Rampello, S.E. Glynn, Dissecting substrate specificities of the mitochondrial AFG3L2 protease, Biochemistry 57 (2018) 4225–4235, https://doi.org/10.1021/acs.biochem.8b00565.
[50] J.M. Miller, A.L. Lucius, ATPgammaS competes with ATP for binding at domain 1 but not domain 2 during ClpA catalyzed polypeptide translocation, Biophys. Chem. 185 (2014) 58–69, https://doi.org/10.1016/j.bpc.2013.11.002.
[51] M.A. Tayeh, M.A. Marletta, Macrophage oxidation of L-arginine to nitric oxide, nitrite, and nitrate. Tetrahydrobiopterin is required as a cofactor, J. Biol. Chem. 264 (1989) 19654–19658.
[52] C. Waszczak, et al., Oxidative post-translational modifications of cysteine residues in plant signal transduction, J. Exp. Bot. 66 (2015) 2923–2934, https://doi.org/10.1093/jxb/erv084.
[53] T. Hiratsuka, New ribose-modified fluorescent analogs of adenine and guanine nucleotides available as substrates for various enzymes, Biochim. Biophys. Acta 742 (1983) 496–508.
[54] E. Mossessova, C.D. Lima, Ulp1-SUMO crystal structure and genetic analysis reveal conserved interactions and a regulatory element essential for cell growth in yeast, Mol. Cell 5 (2000) 865–876.